Modeling of SAM Impedance onto Gold and Silver Thin-film Mass-produced Electrodes and Their Use for Optimization of Lactic Acid Detection

G. Rosati, M. Scaramuzza, E. Pasqualotto, A. De Toni, C. Reggiani, and A. Paccagnella, *Member, IEEE*

***Abstract*— In this work, we demonstrate how an innovative, out-of-cleanroom customized CD/DVD fabrication process can be successfully used for mass production of biosensors with thin-film electrodes. We show that silver and gold electrodes can be used for impedimetric and voltammetric biosensing applications, both in presence and absence of a redox mediator. We modeled the redox/non-redox electrodes impedance through equivalent electrical circuits, and we evaluated their transfer function sensitivity with a one-factor-at-a-time approach. Using this approach, we introduced a new prediction method to find which equivalent electrical circuit elements contribute more to the transfer function variations, then we experimentally validated the predictions measuring the electrodes electrochemical impedance spectroscopy responses with relevant self-assembled monolayer molecules immobilized on them, i.e. MCH and DTSP. We also assess the silver electrodes long-term stability with impedance spectroscopy measurements over a period of 1200 hours, proving their possible use in point-of-care applications. Finally, we also prove that the sensors correctly perform in a practical case, i.e., as a lactic acid biosensor, by studying the optimization of the biosensor efficiency through different enzyme immobilization methods. By comparing lactate oxidase enzyme direct adsorption and covalent binding to DTSP self-assembling monolayers, we found that covalent binding to DTSP can boost the catalytic current of about 40% with respect to that obtained from the direct adsorption of the same enzyme concentration.**

***Index Terms*—electrochemical impedance spectroscopy; biosensors; self assembled monolayers; modeling; enzymes; lactic acid**

I. Introduction

Self-assembling monolayers (SAMs) consist of molecules, which may autonomously form uniform layers over flat surfaces. SAMs are usually composed by methylene chains: typically, the tail group shows a high affinity with the substrate material, e.g., thiol group for covalent binding on metals [1, 2]. Conversely, the head group determines the chemical/physical properties of the new self-assembled surface [3, 4]. SAMs [5, 6] are extensively used for biosensing, e.g., to bind biological materials such as proteins, enzymes, and DNA [7] to metal surfaces, to promote a particular orientation of DNA chains [8], or to change the sensor surface properties to promote or prevent the cell binding [9].

SAMs are also used as uniform surface spacers to immobilize enzymes onto the electrodes and prevent their unfolding, as in case of Dithiobis n-succynimidil propionate SAM (DTSP) for the lactate oxidase enzyme (LOx) immobilization [10].
This strongly affects the biosensor performance and reproducibility [11], as enzymes are proteins whose peculiar spatial fold promotes catalysis, and thus unfolding events related to temperature, pH, ionic strength, and also immobilization method [12, 13], can cause enzymes to lose catalytic activity efficiency. This approach allows for the improvement of the sensitivity of this kind of sensors for the detection of relevant molecules as lactate and glucose. These molecules have attracted a lot of attention due to their relation to widespread diseases [14], such as diabetes and hypoxia [15], and to food and beverages contaminations [16]. Several strategies were adopted to detect such molecules in different samples like blood, urine or tear fluid [17], and also in cells and tissues [4, 14].

In order to optimize the SAM immobilization process, the manufacturing of flat metal surfaces with a low amount of impurities is fundamental for the SAM uniformity and it strongly affects the biosensor performance, e.g., its sensitivity and detection limits. Two common metal deposition techniques are evaporation and plasma-sputtering. With the former technique, metal is deposited in vacuum by thermal evaporation from a crucible, while in the latter, a metal target undergoes a plasma bombardment and the ejected atoms form a metal thin-film. The plasma-sputtering allows for higher device throughput since it doesn't need the heating of the metal. The

This work has been partially supported by Myo-Screen project (PSR Veneto 2007-2013 Misura 124, Veneto region).

G. Rosati, M. Scaramuzza, E. Pasqualotto, A. De Toni, and A. Paccagnella are with the Department of Information Engineering, University of Padova, via Gradenigo 6/b, 35131 Padova, Italy (e-mail: rosatigi@dei.unipd.it, scaramuzza@dei.unipd.it, elisabetta.pasqualotto@unipd.it, alessandro.detoni@dei.unipd.it alessandro.paccagnella@dei.unipd.it)

A. De Toni is also with Next Step Engineering s.r.l., via Newton 36, 35131 Padova, Italy (e-mail: info@nextstepsrl.it)

C. Reggiani is with the Department of Biomedical Sciences, University of Padova, via U. Bassi 58, 35131 Padova, Italy (e-mail: carlo.reggiani@unipd.it)

industrial process adopted for the manufacturing of the devices used in this work takes advantage of two key features: the fast and reliable molding of flat plastic substrates and a high-energy plasma-sputtering for metal deposition with finely controllable thickness. By combining these two steps, it is possible to successfully manufacture electrodes suitable for the immobilization of different SAM molecules.

Several optical and electrochemical electrodes characterization methods are available. A fast and reliable technique to study the electrode properties, and thus the immobilized SAMs, is the Electrochemical Impedance Spectroscopy (EIS) [18, 19]. The setup is based on electrodes in contact with suitable electrolyte solutions. The impedance of this system is measured in a proper frequency range, modeled, and fitted by different Equivalent Electrical Circuits (EECs). For affinity and enzyme-based biosensors, impedance data modeling is an important part of EIS data analysis as it enables the characterization of molecular binding events, using lumped, pseudo-distributed or distributed element models [20, 21]. The specific EEC topologies allow for investigating different surface phenomena, e.g., sensor coverage with immobilized SAMs [5], antibodies [22], or DNA [23].

The presence of a redox mediator in the testing solution, i.e., the measuring sample in affinity EIS-based sensors, is not always possible: in facts, it can induce electrodes surface alterations (e.g., electrodes oxidation) and modification of their conductivity (as in the case of many polymeric electrodes [24]) that nullify the measurements results. However, we will show that it is possible to find proper EEC topologies and elements that are sensitive to the electrodes surface status even in absence of redox mediator.

II. Materials and Methods

A. Reagents and enzyme immobilization

All the reagents used in this work were provided by Sigma-Aldrich. Deionized water was used to dissolve previously weighted Phosphate Buffered Saline (PBS) powder pouches, producing PBS 100 mM pH 7.4. PBS was used to dilute ferricyanide and ferrocyanide. The redox mediator used for the EIS measurements was then prepared by mixing equal volumes of ferricyanide 2 mM and ferrocyanide 2 mM, obtaining ferro/ferricyanide 1 mM. The non-redox mediator used for the EIS measurements was KH_2PO_4 100 mM pH 7.4.

Regarding the SAMs, mercapto 1-hexanol (MCH) powder was diluted in milliQ water, then aliquoted and stored at 4 °C. Dithiobis n-succynimidil propionate (DTSP) solutions were diluted in dimethyl sulfoxide (DMSO) 10 %, aliquoted, and then stored at -20°C. The enzyme for lactate detection, i.e., lactate oxidase (LOx) from Pediococcus sp. in powder form (100 units), was diluted in Phosphate Buffered Saline (PBS), aliquoted, and stored at -20°C. Since the Sigma-Aldrich supplied LOx quantity is specified in enzymatic units (U), all the enzyme dilutions in the following will be indicated in U/ml. The product specification sheet declares just that the enzyme activity is ≥ 20 U/mg. Therefore, the effective enzyme concentration in mg/ml can be only upper limited by the concentration values in U/ml divided by 20.

The LOx enzyme immobilization was performed in two different ways, i.e., by simple adsorption on the electrode surfaces, and by covalent binding on previously DTSP functionalized electrodes. The immobilization by simple adsorption was achieved by drop-casting 1 µl of the LOx solution over the working electrode surface and rinsing the surface with PBS after 1 hour, to remove excess enzymes. Conversely, the LOx covalent binding was performed using the same protocol on electrodes previously functionalized by drop-casting DTSP and rinsing after 3 hours.

B. Devices and electrodes

The devices used in this work were produced with a modified CD/DVD industrial process (Next Step Engineering s.r.l., Italy) based on a Skyline Replication Line (Singulus Technologies) with integrated injection molding and plasma sputter stages. The new patented features [25] enables mass-production of electronic devices with sub-mm feature size, suitable for biomedical and biological applications, with high reproducibility of surface features and custom metal patterns. All the manufacturing steps are inherently automated, starting from the plastic substrate molding to the high-speed, high-power metal deposition for the electrodes pattern. All the fabrication parameters, e.g., electrodes metal thickness and molding temperature, can be adjust through the machine in-built control system, without any direct intervention of the operator in the manufacturing process. The devices were embedded in discs made of flat optically neutral polymeric substrates, with a thin metallization, and a screen-printed insulating layer to pattern the square electrodes.

We previously tested the optical and electrochemical properties of such electrodes for SAM studies with good results [26]. In this work, the resulting working electrodes are 1 mm wide, with a 50 nm thick silver or gold metal layer (average roughness R_a of 1-2 nm), over a 0.6 mm thick optically neutral polycarbonate substrate. With this electrodes geometry, we created about 200 working electrodes on the same disc, with a production rate of 1 disc every 30 seconds. Depending on the adopted metal pattern, the electrodes manufacturing throughput can be speed up to about 25 full electrodes per second. To complete the electrochemical cell, we drop-casted the electrolyte solutions directly onto the working electrode, 50 µl volume for each test, then the reference electrode (CH111, CH Instruments Ag/AgCl electrode in KCl 1 M, and the counter electrode (CHI129, CH Instruments platinum wire) were immersed into the resulting drop.

C. EIS measurements setup

We performed the EIS measurements in the 1 Hz – 100 kHz frequency range, by applying an AC voltage of 10 mV peak to peak, using a Solartron 1260 impedance analyzer (Solartron) with a custom LabView (National Instruments) software to drive the instrument. We used Matlab R2009a (The MathWorks) to analyze EIS data. We also used ZView 3.3a (Scribner Associates Inc.) software to fit EIS data, assess fits goodness, and evaluate equivalent parameters identification errors.

D. Modeling

The modeling of the electrodes impedance data is based on the EECs showed in Fig.1, depending on the electrolyte which is used.

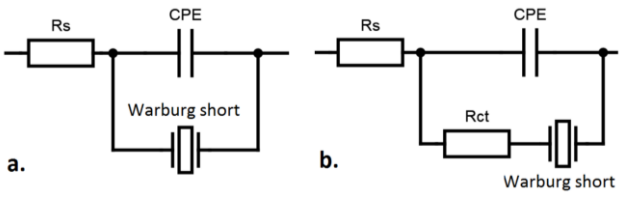

Fig. 1.Equivalent Electrical Circuits (EECs) used to model the mediator-free impedance data (a) and the redox mediator-based ones (b).

Electrochemical systems consisting in redox mediator-free electrolytes are usually modeled by the series of a resistor and a Constant Phase Element (Fig. 1a), which is defined as:

$$Z_{CPE} = C^{-1}(j\omega)^{-n} \quad (1)$$

where ω is the angular frequency measured in radians per second, C a capacitance value, and n a real number between 0 and 1. In this EEC (Fig. 1a), the resistor accounts for the conductance of the electrolyte (solution resistance, R_s), while the *CPE* is related to the electrodes surface characteristics.
Conversely, the electrochemical systems characterized by a redox mediator (Fig. 1b) are usually modeled by the same EEC previously described, adding a resistor in parallel with the *CPE*. This resistor accounts for the charge transfer between the electrodes through the redox mediator, thus is called R_{ct} [27].

In this work, the gold and silver electrodes impedance data have been modeled with the EECs shown in Fig. 1, adding to the EECs previously described, a Warburg short element (W_s) in parallel with *CPE*. This element accounts for the diffusion of the electrolytes charges from and to the electrodes and is defined as:

$$Z_{Ws} = A\frac{tanh(bj\omega)^d}{(bj\omega)^d} \quad (2)$$

where A is a constant impedance and b and d real numbers.

Each SAM coverage has been tested over at least 3 different electrodes. Their impedance spectra have been averaged and the mean values have been used for the fitting. The data points weight has been normalized by their magnitude for the Zview fitting, with its proprietary method. The errors estimations for the EECs parameters values are calculated by testing several solutions near the "best fit" and checking which parameter variation results in a significant decrease of the fit goodness (g_{fit}). Therefore, defining P_0=(p_{01}, ..., p_{0M}) the vector of the EEC's parameters values (p_i) obtained by the "best fit", the error ϵ_i^{err} on parameter p_i is the maximum value which, added to p_{0i}, didn't cause any g_{fit} variation (3).

$$\epsilon_i^{err} = \max[\epsilon_i : g_{fit}(p_{01}, \dots, p_{0i} + \epsilon_i, \dots, p_{0M}) = g_{fit}(p_{01}, \dots, p_{0i}, \dots, p_{0M})] \quad (3)$$

With the purpose to theoretically evaluate the best EEC parameters describing the electrodes surface covered by the immobilized SAMs, we introduce a numerical method allowing to estimate the effect of each parameter on the EEC's transfer function, i.e. the transfer function sensitivity to each parameter variations.
This method uses the Normalized Residual Sum of Squares (NRSS) concept, as shown in the following paragraph, applied to the impedance module and phase of the EECs of Fig. 1. Within this approach, the SAM covered electrode's impedance has been fitted by the proper EEC, obtaining the "best fit" (p_{0i}) parameters values. Then, the NRSS has been used to find the parameter p^*, whose alteration causes the maximum transfer function variation.

The single parameters have been randomly varied One-At-a-Time (OAT approach) [28] in the range between ±50 % of p_{0i}, obtaining random p values and thus P vectors. Then, the NRSS has been calculated in (4) and (5) for the impedance module and phase, respectively.

$$NRSS_{module} = \sum_{i=1}^{N}\left(\frac{[|Z_{meas}(f_i)|-|Z(f_i,P)|]^2}{[|Z_{meas}(f_i)|-|Z(f_i,P_0)|]^2}\right) \quad (4)$$

$$NRSS_{phase} = \sum_{i=1}^{N}\left(\frac{[\langle Z_{meas}(f_i)\rangle-\langle Z(f_i,P)\rangle]^2}{[\langle Z_{meas}(f_i)\rangle-\langle Z(f_i,P_0)\rangle]^2}\right) \quad (5)$$

Defining f = (f_1, ..., f_N) the vector of the frequencies, $Z_{meas}(f_i)$ is the measured impedance correspondingly to the f_i frequencies. Conversely, $Z(f_i,P)$ is the EEC transfer function calculated with the f_i frequencies and the p_i parameters values, while $Z(f_i,P_0)$ is calculated with the parameter values obtained by the data fitting p_{0i}. Finally, $|Z|$ and $\langle Z\rangle$ represent the magnitude and phase of the transfer function, respectively.

III. Results and Discussion

A. Silver electrodes

We characterized the silver electrodes surface coverage with EIS after MCH immobilization with overnight drop-casting protocol and subsequent electrodes washing with MilliQ ultrapure water to remove unspecifically bound MCH molecules. Eight MCH concentrations, ranging from 10 nM to 1 mM, were prepared and immobilized onto 24 electrodes. We performed the EIS measurements in 100 mM potassium phosphate monobasic buffer, with a DC bias of 0 V.

Fig. 1a shows the EEC used to model the silver electrodes electrochemical cell and therefore to fit the EIS spectra for all the immobilized MCH concentrations. The CPE element (1) describes the double layer capacitance of the electrode/electrolyte interface [29], which strongly depends on the surface condition, i.e., on SAM surface coverage. Thus, we introduce the parameter θ_C to describe the surface coverage, involving the CPE element:

$$\theta_C = 1 - \frac{C_f}{C_b} \quad (6)$$

where C_b and C_f are the C values in (1), of the bare (non-functionalized) and functionalized electrodes, respectively, obtained by fitting the EIS data. The relative error on θ_C for each MCH concentration follows the propagation [30] of the C_f and C_b errors $\epsilon^{err}{}_C$ (3), obtained by the fitting software.

This article has been accepted for publication in a future issue of this journal, but has not been fully edited. Content may change prior to final publication. Citation information: DOI 10.1109/TNB.2016.2616194, IEEE Transactions on NanoBioscience

Fig. 2 depicts the NRSS analysis results for the impedance module with the EEC of Fig. 1a. Each plot has been obtained by (4), keeping all the EEC's parameters constant (to their p_{0i} values) but one, which has been varied in a range of ±50 % with respect to its best fit value (OAT approach). In particular, we have applied this method to each electrical parameter, i.e., R_s, C, A, and b, as listed in the inset of the figure. The most significant parameter for the transfer function, which is identified by the maximum NRSS, is the best parameter for describing the surface coverage, producing the widest dynamic range.

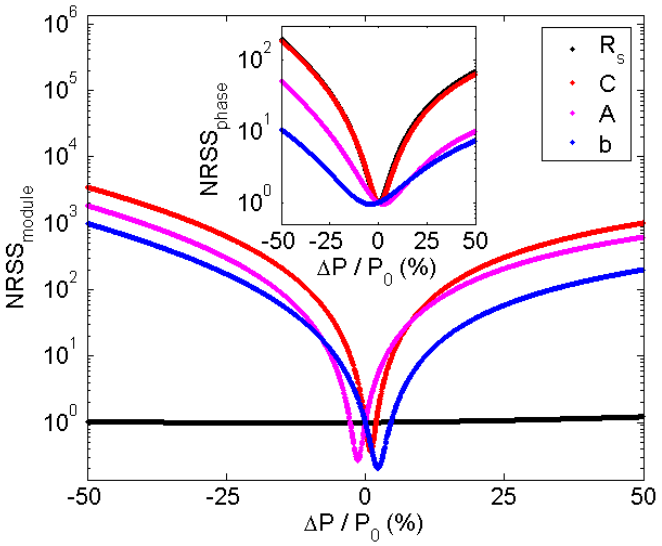

Fig. 2.OAT analysis outcomes for the NRSS of the impedance module of 10 µM MCH SAM-modified silver electrodes modeled with Eq. 6. The inset depicts the NRSS values obtained for the impedance phase of the same data.

From the curves in Fig. 2 it is not straightforward to identify such a parameter, even though C shows the highest value at the limits of the variation range (±50 %). Similar results are found also for $NRSS_{phase}$, which is represented in the inset of the figure, even though the R_s NRSS values are close to the C ones. In order to clearly identify the best parameter, we now consider the average values of the $NRSS_{module}$ and $NRSS_{phase}$ calculated over ±50 % variation range (Table I).

TABLE I
MEAN OF $NRSS_{MODULE}$ AND $NRSS_{PHASE}$ OVER ±50 % VARIATION RANGE FOR EECS PARAMETERS OF FIG. *1A.*

NRSS	NRSS of EEC parameters			
	R_s	C	A	b
$NRSS_{module}$	1.04	708.10	384.54	181.34
$NRSS_{phase}$	42.07	39.64	9.74	3.65

Again, C is the parameter with the maximum impact on the sensitivity of the transfer function. In such analysis, we have not considered the parameters n (1), and d (2), as they have not an explicit or physical-chemical relationship with the electric charge transfer at the electrode surface and with the surface coverage. Furthermore, as they appear as exponent, they would overwhelm the effect of any other parameter variation. Therefore, since C resulted the best parameter from the NRSS analysis, θ_C is a suitable parameter to describe the variations of the electrodes impedance due to the adsorption of molecules onto their surfaces in the redox mediator-free system.

Fig. 3 shows the Nyquist plots of EIS measurements on silver electrodes functionalized with different concentrations of MCH SAMs.

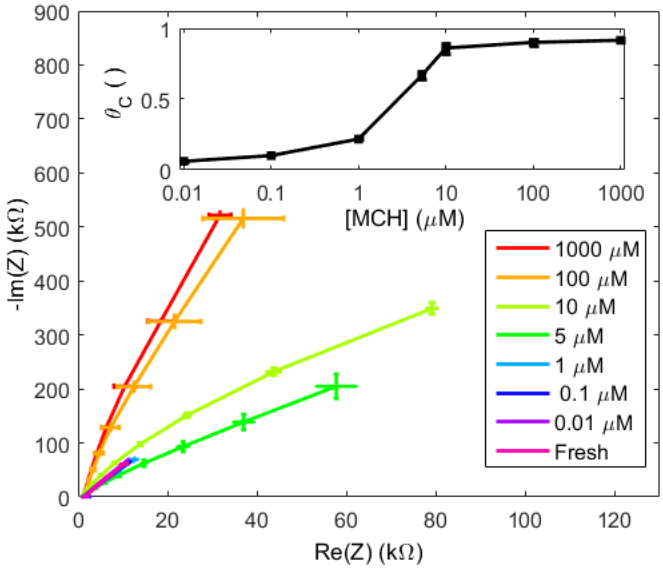

Fig. 3. Nyquist plots of the MCH-modified silver electrodes and θ_C values as a function of MCH concentration (inset).

The increase of the immobilized MCH concentration causes the increase of the double layer capacitance impedance, denoted by higher impedance values, and by an increase of the linear Nyquist plots' slope at the highest concentrations. The correspondent values for θ_C as a function of MCH concentration, shown in Fig. 3 inset, exhibit a sigmoid behavior with two plateaus. For low MCH concentration θ_C is below 0.1 and, since the variations of $|Z|$ from the bare condition are small (Fig. 3), this suggest that the electrode's coverage is very limited with these concentrations. Conversely, for high MCH concentrations, θ_C reaches values slightly above 0.9 and this correspond to the saturation of the $|Z|$ variations (Fig. 3). As can be seen in Fig. 3 inset, in the concentration region between the two plateaus, i.e., from 1 to 10 µM, θ_C increases about 3 times, indicating the progressive coverage of the electrode surface by the MCH SAM. At low concentrations θ_C increases by about 68.0 +/- 1.8 % when the SAM concentration grows from 10 nM to 100 nM. Hence, in this region we may effectively measure small concentration variations. These estimation errors increase to about 2 % at higher concentrations, with a maximum of about 4.5 % in the transition region between the two plateaus.

Therefore, EIS measurements with MCH proved the feasibility of silver devices for affinity biosensing purposes. However, silver electrodes exhibited severe surface alterations in presence of redox mediators as ferro/ferricyanide and showed severe surface modifications with the application of positive DC potentials. These characteristics don't allow the usage of these devices for enzyme-based biosensors.

Therefore, in order to further the silver electrodes surface properties, the stability of the electrodes over time was tested in a redox mediator-free system using EIS measurements. We

This article has been accepted for publication in a future issue of this journal, but has not been fully edited. Content may change prior to final publication. Citation information: DOI 10.1109/TNB.2016.2616194, IEEE Transactions on NanoBioscience

characterized both bare and 1 mM MCH functionalized silver electrodes for a period of about 1200 hours. 96 electrodes, 48 bare, and 48 MCH-functionalized were prepared in sealed Petri dishes (4 for each dish) and kept at 4°C. Four bare and four functionalized electrodes were tested for each period of time, from 3 hours until 50 days after the preparation.

Fig. 4 shows the θ_C values for the tested electrodes over 1200 hours.

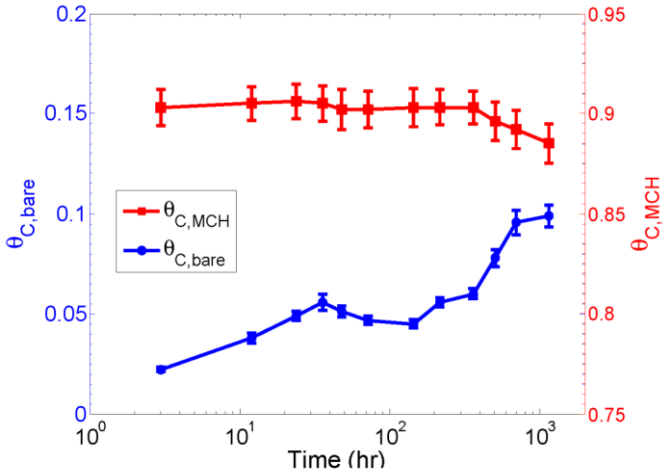

Fig. 4. Stability of 1 mM MCH-modified silver electrodes. Coverage parameters θ_C for bare (blue •) and functionalized (red ▪) silver electrodes are reported as a function of time. Lines connecting the points are drawn to guide the eye.

For periods within 17 days, θ_C values for bare electrodes are lower or similar to those previously obtained for 10 nM MCH functionalization (0.06 with 1.7 % error), indicating that no major modifications take place on the stored electrodes; for longer periods, θ_C reaches values similar to 100 µM MCH. Conversely, θ_C values for MCH-functionalized electrodes are higher than 0.875, i.e., the 1 mM MCH functionalization layer is stable enough to last 50 days in the tested conditions. Furthermore, the mean θ_C value for MCH-modified electrodes evaluated on the entire storage period is 0.9004 with 0.7 % standard deviation (SD), which is in good compliance with θ_C value obtained from the coverage study for 1 mM MCH functionalization, i.e., 0.916 with 1.5 % error. Therefore, we proved that in both cases the silver electrode can resist or even avoid the surface oxidation by appropriately choosing both the immobilization protocol, the devices conservation method, the EIS measurements solution, and the applied measurement voltage.

B. *Gold electrodes*

For gold electrodes we immobilized five concentrations of DTSP solutions, from 100 nM to 1 mM in DMSO 10 %, by drop-casting for 3 hours and washing the electrodes in DMSO 10% to remove the unspecific bound DTSP molecules. We characterized the obtained SAMs with EIS measurements in 1 mM ferro/ferricyanide in PBS 100 mM, by applying a DC bias of 236 mV.

This electrochemical system is well described by the EEC of Fig. 1b. The R_{ct} is related to the charge transfer process at the electrode interface. Similar to what made with *CPE*, we introduce the parameter θ_R, involving R_{ct}.

$$\theta_R = 1 - \frac{R_{ct,b}}{R_{ct,f}} \tag{7}$$

where $R_{ct,b}$ and $R_{ct,f}$ are obtained from the EIS data of the bare (non-functionalized) and functionalized electrodes, respectively. Again, the relative error on θ_R parameter for each DTSP concentration follows the propagation [30] of the R_{ct} errors $\epsilon^{err}{}_{Rct}$ (3), obtained by the fitting software.

Fig. 5 shows the NRSS analysis results for the impedance module in the case of the mediator-based system, which EEC is represented in Fig. 1b.

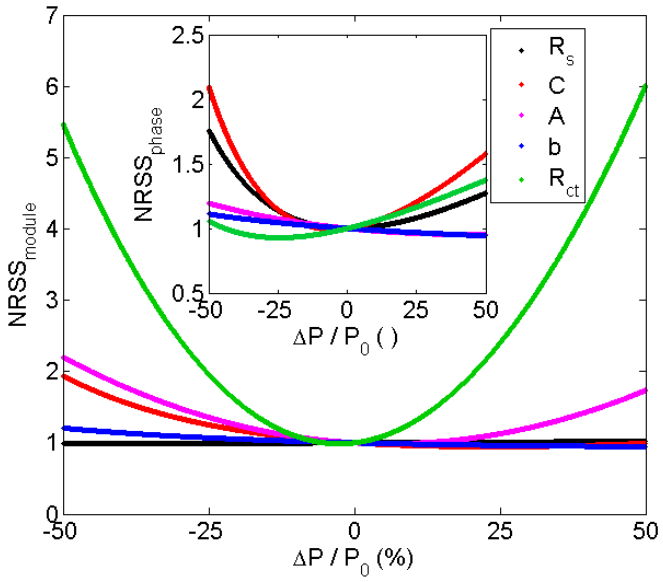

Fig. 5. NRSS analysis for 100 µM DTSP SAM-modified gold electrodes impedance module. The inset depicts the NRSS analysis for the phase of the impedance.

A new electrical parameter has been introduced with respect to the mediator-free (EEC of Fig. 1a) NRSS analysis, i.e., R_{ct}. This parameter variation in the ±50 % range result clearly in the maximum $NRSS_{module}$ values, followed by the C parameter. Conversely, the results obtained with the $NRSS_{phase}$ (represented in the figure inset) show that the C parameter NRSS dominates over the other parameters one. Also in this analysis the parameters n and d have been excluded, since the same considerations made within the silver electrodes NRSS analysis remain valid.

The average values of $NRSS_{module}$ and $NRSS_{phase}$ reported in Table II, and calculated over ±50 % variation range, confirm that R_{ct} has the maximum influence on the transfer function module of Fig. 1b EEC.

TABLE II
MEAN OF $NRSS_{MODULE}$ AND $NRSS_{PHASE}$ OVER ±50 % VARIATION RANGE FOR EECS PARAMETERS OF FIG. *1B.*

NRSS	NRSS of EEC parameters				
	R_s	C	A	b	R_{ct}
$NRSS_{module}$	1.00	1.14	1.32	1.03	2.57
$NRSS_{phase}$	1.16	1.25	1.02	1.01	1.07

Therefore, θ_R is a suitable parameter for the gold electrode's surface description. However, the *C* parameter seem to have a significant influence on the transfer function also in this case.

Fig. 6 shows the EIS results for DTSP SAM immobilization on gold electrodes.

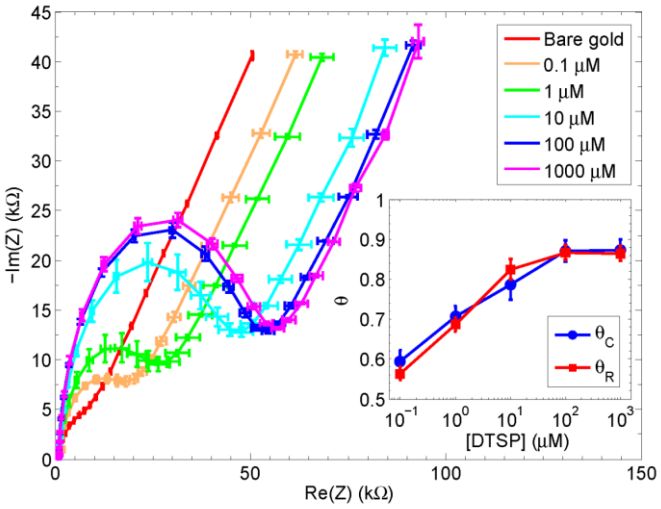

Fig. 6. Nyquist diagrams of the EIS measurements of DTSP-modified gold electrodes at the different concentrations and comparison between different coverage parameters, i.e., θ_C and θ_R (inset).

As expected, the diameter of the high frequency semi-circle increases with DTSP concentration, corresponding to an increase of the R_{ct} value [19].

We fitted these datasets with Fig. 1b EEC, obtaining the surface coverage parameters θ_C and θ_R depicted in Fig. 6 inset as a function of the immobilized DTSP concentration. The minimum DTSP concentration giving the maximum surface coverage is 100 µM, that corresponds to θ_R = 0.87 (2.1 % error).

As can be observed in Fig. 6 inset, θ_R and θ_C parameters have similar behaviors, showing a plateau for concentrations higher than 10 µM DTSP. In correspondence to these concentrations the Nyquist diagrams of Fig. 6 saturate, thus it's probable that the electrode surface has been completely covered by DTSP.

Interestingly, even with the lowest DTSP concentration, i.e. 100 nM, both θ_R and θ_C show fairly high values in Fig. 6 inset, i.e., θ_R=0.56 (3 % error) and θ_C=0.59 (4.5 % error), indicating an higher electrode's surface coverage than what was expected from the low DTSP molecules molecular weight. This is probably due to the homo-bifunctional structure of DTSP, which has two N-hydroxysuccinimide esters at the ends of two spacer arms connected by a disulfide group. This structure could promote the binding of the DTSP molecules in a planar configuration onto the electrode surface at low concentrations, causing a residual surface coverage higher than the one associated to the vertical configuration, as for MCH [31].

IV. Applications: Lactic Acid Detection Efficiency Enhancement by Immobilization Optimization

Gold is a typical substrate for the implementation of mediator-based lactic acid electrochemical biosensors [10, 32, 33]. Several functionalization strategies can be used for the enzymes immobilization onto the electrode surface: the easiest one is direct adsorption, which is a non-covalent binding. Hence, we investigated the direct adsorption of Lactate Oxidase (LOx) enzymes over gold electrodes using EIS measurements for different concentrations of LOx solutions in PBS. Fig. 7 shows the Nyquist diagrams of the LOx-modified electrode's impedance.

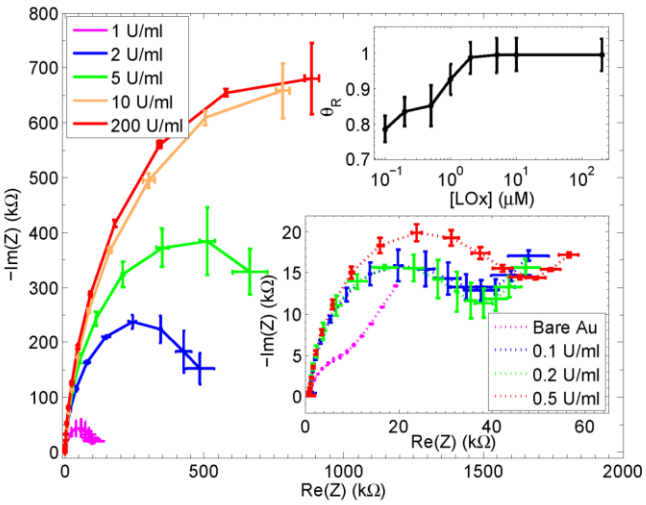

Fig. 7. Nyquist diagrams of the EIS measurements of LOx-modified gold electrodes and θ_R values as a function of LOx concentration (top inset). The bottom inset show a magnification for lower tested concentrations.

For LOx concentrations below 1 U/ml (represented in the Fig. 7 bottom inset), the diagrams present a charge transfer related semicircle and a linear part, related to the low-frequency diffusion component [34]. Increasing the LOx concentration, the diffusion part is overwhelmed by the semicircles as the charge transfer barrier at the electrode surface increases.

We have then evaluated the electrodes coverage parameter θ_R, previously introduced, by fitting the impedance data with the EEC shown in Fig. 1b. The R_{ct} values obtained from the fitting procedure vary over more than two orders of magnitude between the bare gold electrode's surface and 200 U/ml LOx, as inferred from the charge transfer semi-circle radius of the Nyquist diagrams. Fig. 7 top inset shows the θ_R values, which are higher than 0.75 for all the tested concentrations and present a plateau at 1 for LOx concentrations above 2 U/ml; for contrast, the Nyquist plots are strongly different up to 10 U/ml. This strikingly different behavior is due to the values of the parameters defining θ_R. In particular, R_{ct} in the bare electrode condition is pretty small in comparison with $R_{ct,f}$: for LOx concentrations over 2 U/ml, the ratio $R_{ct,b}/R_{ct,f}$ becomes so tiny that θ_R is practically 1, independently of the actual R_{ct} values, which instead strongly control the Nyquist behavior in Fig.7.

We used the non-covalently LOx-modified gold electrodes for the detection of L-(+) lactic acid (LA) by Differential Pulse Voltammetry measurements (DPV), in the same solution used for the EIS measurements, with 1 mM LA.

The LA detection is based on the catalysis mediated by the LOx enzyme, which converts lactic acid into pyruvic acid, and molecular oxygen in hydrogen peroxide, in stoichiometric ratio. As sketched in Fig. 8, the presence of ferricyanide in solution allows the hydrogen peroxide to be converted back to oxygen reducing the ferricyanide molecules to ferrocyanide. Then,

ferrocyanide is oxidized back to ferricyanide at the electrode surface during the DPV measurements, producing a detectable current proportional to the LA concentration.

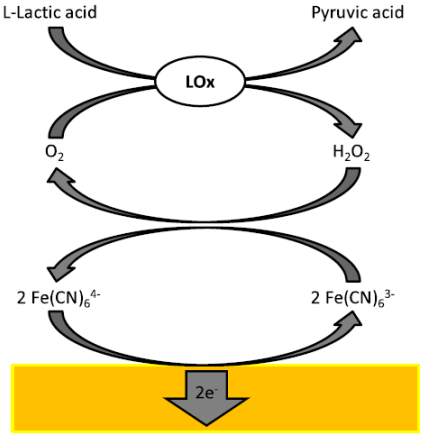

Fig. 8. Scheme of the electrochemical reactions involved in the Lactic acid catalysis mediated by the LOx enzyme and in the ferro/ferricyanide-mediated voltammetric detection at the electrode (on the bottom).

The correlation between the LA concentration and the recorded current through the LOx enzyme reaction has been previously characterized and verified with the same setup and on the same type of electrodes by Cyclic Voltammetry (CV) measurements [35].

In our experiments, we performed the DPVs in the range between 0.05 V and 0.45 V, with amplitude of 50 mV and pulse width and period of 0.2 s and 0.5 s, respectively. The current has been sampled before each pulse.

In order to evaluate the LA sensitivity of our electrodes, we have performed DPV measurements on the non-covalently LOx-modified electrodes for two solutions, i.e., one with 1 mM LA and one by replacing LA with PBS. The DPV measurements resulted in both cases bell-shaped, and therefore we used the peak current values ($i_{p,LA}$ and $i_{p,PBS}$, respectively) to detect LA. Hence we introduce (8) the perceptual variations of the DPV peak currents (Δi_p) in presence of LA with respect to that obtained with PBS:

$$\Delta i_p = 100 \frac{i_{p,LA} - i_{p,PBS}}{i_{p,PBS}} \quad (8)$$

In Table III we list the Δi_p values as a function of the immobilized LOx concentration.

TABLE III
PERCENTAGE VARIATIONS OF DPV PEAK CURRENTS FOR LOX DIRECT ADSORPTION.

[LOx] (U/ml)	0.1	0.2	0.5	1	2	5
Δi_p (%)	0.92	8.23	19.01	15.80	20.92	5.07

The larger Δi_p values, around 20%, appear for a LOx concentration between 0.5 and 2 U/ml, where also θ_R increases. In fact, the enhancement of Δi_p is related to the electrode surface coverage: the amount of enzyme adsorbed over the electrodes can effectively catalyze the reaction with the LA solution, and increasing the LOx concentration above 0.5 U/ml does not affect the amperometric response [36] up to 2 U/ml. The drop in Δi_p for 5 U/ml LOx is likely due to fully covered electrodes with disorderly adsorbed enzymes layers, as suggested by the high semicircle radius of the Nyquist diagrams in Fig. 7. In this case, non-optimal molecular arrangements may effectively decrease the lactate catalysis efficiency.

Even though we have identified (Table III) the optimum interval of LOx concentrations, the current variations are quite small for the reliable detection of 1 mM LA. Since this could be due to directly adsorbed enzyme unfolding, as verified by Szucs et al. with Glucose Oxidase [37], we aimed to reduce this problem by preparing new gold devices with covalently immobilized LOx over the DTSP SAM previously presented. We selected the LOx concentration of 0.5 U/ml, since it is the lowest concentration generating the maximum Δi_p, and 200 U/ml, which is the highest LOx concentration we tested. Then, we drop-casted them over gold electrodes functionalized with DTSP at five different concentrations, ranging from 0.1 to 1000 mM, one per decade. We performed EIS measurements and fitted the impedance data, to obtain the R_{ct} and the θ_R values for the DTSP/LOx-modified electrodes, reported in Fig. 9.

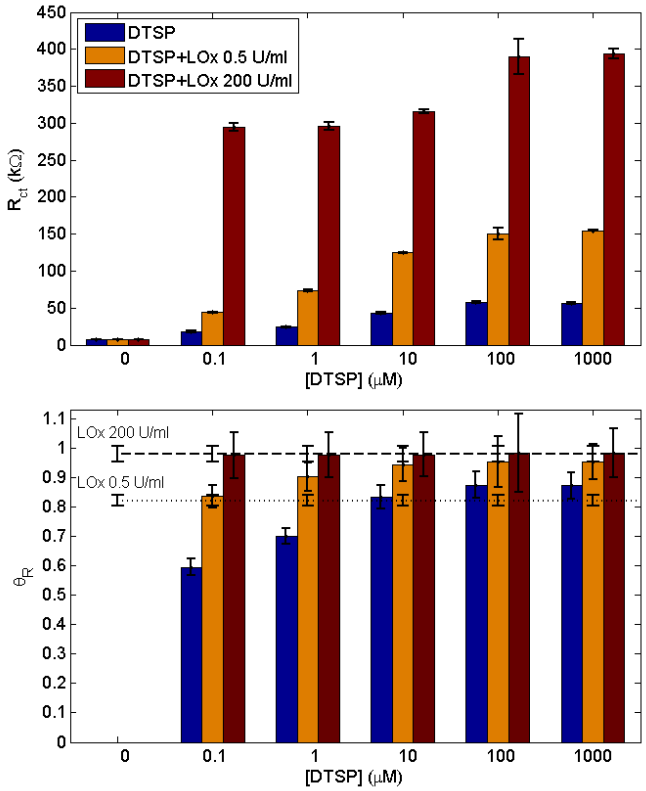

Fig. 9. Effect of LOx covalent binding on R_{ct} (top plot) and on θ_R values (bottom plot) as a function of DTSP concentration for gold electrodes. As a comparison, θ_R values for two concentrations of directly adsorbed LOx onto gold electrodes are depicted (taken from Fig. 10): 0.5 U/ml (dashed line), 200 U/ml (dotted line).

At LOx 0.5 U/ml, R_{ct} and θ_R values grow with DTSP concentration, as in case of DTSP-modified electrodes without LOx, and their higher values are consistent with more molecules bound at the DTSP SAM surface [10]. Moreover, the immobilized DTSP concentration affects the overall θ_R values: for low DTSP concentrations, θ_R corresponds to that of directly adsorbed 0.5 U/ml LOx, i.e., about 0.83 (see the dashed line in

Fig. 9), while for higher concentrations the coverage parameter values reach 0.95.

At 200 U/ml LOx, the θ_R values result independent from DTSP concentration, even though a variation in the R_{ct} plot is observed. This is probably due to the huge variation of the R_{ct} values obtained with the immobilization of high enzyme concentrations which cause the $R_{ct,b}/R_{ct,f}$ to be very close to zero and thus the θ_R values to be approximatively equal to 1. This fact partially masks the DTSP effect. In fact, θ_R values for DTSP/LOx-modified electrodes are similar to that obtained with LOx 200 U/ml directly adsorbed on the electrodes (see dotted line in Fig. 9).

We performed DPV measurements on DTSP/LOx-modified electrodes with the same protocol previously used (Fig. 9), both in 1 mM L-(+) LA and PBS. Fig. 10 shows the variations between the LA and PBS DPV measurements with LOx directly adsorbed onto the electrode, and covalently bound to DTSP SAM.

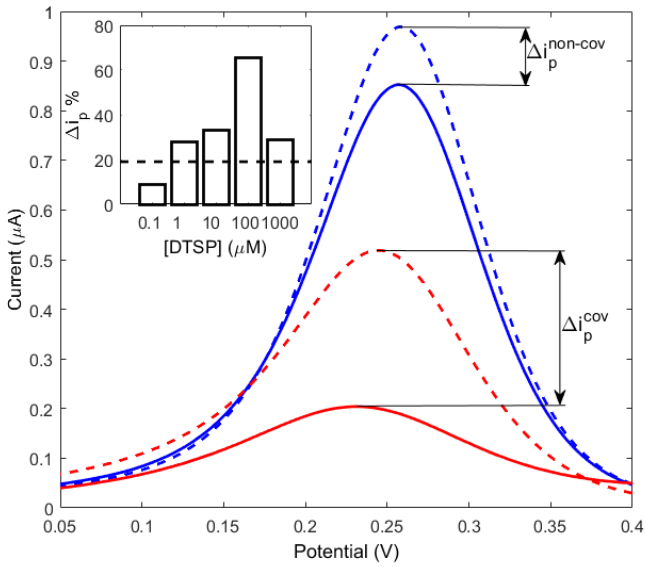

Fig. 10. DPV measurements on modified gold electrodes with LOx 0.5 U/ml non-covalently bound onto the electrode (blue), and covalently bound to DTSP 100 μM (red) in absence (continuous lines) and in presence (dashed lines) of 1 mM LA. Inset: percentage DPV peak currents variations due to LA detection with covalently LOx-modified electrodes compared to the Δi_p obtained by the non-covalently LOx-modified ones (dashed line).

As expected, the DPV peak currents associated to DTSP/LOx-modified electrodes are lower than the non-covalently LOx-modified ones. This is due to the higher R_{ct} values of these electrodes with respect to the LOx-modified ones.

Table IV and Fig. 10 inset show the resulting Δi_p percentage variations as a function of DTSP concentration. Δi_p values are higher than in case of directly adsorbed LOx (dashed line in Fig. 10 inset) when the DTSP concentration is ≥1 μM, with a peak value of 66 % for 100 μM DTSP.

TABLE IV
PERCENTAGE VARIATIONS OF DPV PEAK CURRENTS FOR COVALENTLY BOUND 0.5 U/ML LOX

[DTSP] (μM)	0.1	1	10	100	1000
Δi_p (%)	8.86	28.02	33.17	65.80	28.32

The covalent binding with DTSP enables higher enzymatic reaction and consequent increase in the current detected by the electrochemical cell. This suggests that a SAM able to effectively bind LOx onto gold can be obtained for DTSP concentrations lower than 1 mM, by using the adopted functionalization protocol.

V. CONCLUSION

In this work we presented mass-produced thin-film electrodes manufactured with a modified CD/DVD industrial process and we proved their feasibility in biosensing applications. In particular, we modeled and studied gold and silver electrodes coverage by SAM molecules through EIS measurements.

We theoretically studied the adopted equivalent models using a new method, based on Normalized Residual Sum of Squares (NRSS), that allowed to identify the model transfer functions dominating parameters by an OAT approach. These parameters were selected to describe the gold and silver electrode surfaces status.

The validity of these parameters as electrode surface status descriptors was experimentally assessed by EIS measurements after the immobilization of different SAM concentrations (MCH for silver and DTSP for gold electrodes).

Moreover, to prove the silver electrodes resistance to oxidation and surface alterations, they were tested both in the bare and in the MCH functionalized conditions, for a period of more than 1000 hours. A minimum duration of 17 days without major surface modifications was proved for bare silver electrodes, meanwhile MCH-functionalized ones showed a 50 days long life.

To prove the validity of these electrodes in the biosensor field, we used gold electrodes to study a typical topic for electrochemical sensors, i.e., the enhancement of the lactic acid amperometric detection. We compared the current generated in presence of 1mM LA after the covalent binding of LOx enzymes on DTSP SAM, with that one generated by adsorbed enzymes. We found that, in presence of 1 mM LA, the covalent binding of 0.5 U/ml LOx on a 100 μM DTSP SAM can boost the current of about 40 % with respect to that obtained from the adsorption of the same LOx concentration.

REFERENCES

[1] J. C. Love et al., "Self-assembled monolayers of thiolates on metals as a form of nanotechnology," *Chemical Reviews*, vol. 105, no. 4, pp. 1103–69, 2005.

[2] J. C. Hoogvliet, et al., "Electrochemical pretreatment of polycrystalline gold electrodes to produce a reproducible surface roughness for self-assembly. A study in phosphate buffer pH 7.4," *Anal. Chem.*, vol. 72, pp. 2016–2021, 2000.

[3] A. Kudelski, "Structures of monolayers formed from different HS-(CH2)2-X thiols on gold, silver and copper: comparative studies by surface-enhanced Raman scattering," *J. Raman Spectrosc.*, vol. 34, no. 11, pp. 853–862, 2003.

[4] D. Chen and J. Li, "Interfacial design and functionalization on metal electrodes through self-assembled monolayers," *Surf. Sci. Rep.*, vol. 61, no. 11, pp. 445–463, 2006.

[5] M. S. Góes et al., "A dielectric model of self-assembled monolayer interfaces by capacitive spectroscopy," *Langmuir*, vol. 28, no. 25, pp. 9689–99, 2012.

[6] W. Wang et al., "Electric Potential Stability and Ionic Permeability of SAMs on Gold Derived from Bidentate and Tridentate Chelating Alkanethiols," *J. Phys. Chem. C*, vol. 113, no. 9, pp. 3717–3725, 2009.

[7] J. J. Gooding et al., "Parameters important in tuning the response of monolayer enzyme electrodes fabricated using self-assembled monolayers of alkanethiols," *Biosens. Bioelectron.*, vol. 15, no. 5–6, pp. 229–39, 2000.
[8] A. Ferrario et al., "Coadsorption optimization of DNA in binary self-assembled monolayer on gold electrode for electrochemical detection of oligonucleotide sequences," *J. Electroanal. Chem.*, vol. 689, pp. 57–62, 2013.
[9] L. Yan et al., "The interaction of proteins and cells with self-assembled monolayers of alkanethiolates on gold and silver," *Colloids Surfaces B Biointerfaces*, vol. 15, no. 1, pp. 3–30, 1999.
[10] M. Gamero et al., "Nanostructured rough gold electrodes for the development of lactate oxidase-based biosensors," *Biosens. Bioelectron.*, vol. 25, no. 9, pp. 2038–2044, 2010.
[11] B. Lillis et al., "Investigation into immobilisation of lactate oxidase to improve stability," *Sensors Actuators B*, pp. 109–114, 2000.
[12] M. Romero et al., "Design and optimization of a lactate amperometric biosensor based on lactate oxidase cross-linked with polymeric matrixes," *Sensors Actuators B Chem.*, vol. 131, no. 2, pp. 590–595, 2008.
[13] C. Mateo et al., "Improvement of enzyme activity, stability and selectivity via immobilization techniques," *Enzyme Microb. Technol.*, vol. 40, no. 6, pp. 1451–1463, 2007.
[14] A. R. Abdur Rahman et al., "Towards an implantable biochip for glucose and lactate monitoring using microdisc electrode arrays (MDEAs)," *Biomed. Microdevices*, vol. 11, no. 1, pp. 75–85, 2009.
[15] M. Weil and A. Afifi, "Experimental and clinical studies on lactate and pyruvate as indicators of the severity of acute circulatory failure (shock)," *Circulation*, vol. 41, 1970.
[16] R. Monosik et al., "Application of Enzyme Biosensors in Analysis of Food and Beverages," *Food Anal. Methods*, vol. 5, no. 1, pp. 40–53, 2011.
[17] N. Thomas et al., "A contact lens with an integrated lactate sensor," *Sensors Actuators B Chem.*, vol. 162, no. 1, pp. 128–134, 2012.
[18] S. Park, "With impedance data, a complete description of an electrochemical system is possible," *Anal. Chem.*, pp. 455–461, 2003.
[19] J. R. MacDonald and W.R. Kenan, *Impedance spectroscopy - Emphasizing solid materials and systems*, Wiley Interscience, 1987.
[20] M. Scaramuzza et al., "Development of an Electrode/Electrolyte Interface Model Based on Pseudo-Distributed Elements Combining COMSOL, MATLAB and HSPICE," *Procedia Chem.*, vol. 6, pp. 69–78, 2012.
[21] A. Bonyar and G. Harsanyi, "CPE investigation of gold thin films," *Des. Technol. Electron. 1*, pp. 117–120, 2011.
[22] J. Ramón-Azcón et al., "An impedimetric immunosensor based on interdigitated microelectrodes (IDmicroE) for the determination of atrazine residues in food samples," *Biosens. Bioelectron.*, vol. 23, no. 9, pp. 1367–73, 2008.
[23] W. Schuhmann and M. Gebala, "Understanding properties of electrified interfaces as a prerequisite for label-free DNA hybridization detection," *Phys. Chem. Chem. Phys.*, vol. 14, no. 43, p. 14933, 2012.
[24] G. Rosati et al., "Performance Improvement by layout designs of conductive polymer microelectrode based impedimetric biosensors, " *Electroanalysis* vol. 26, pp. 1400-1408, 2014.
[25] A. De Toni, M. Scaramuzza, E. Pasqualotto, "Methods for Lab-On-A-Chip devices manufacturing," Italy Patent VR2013A000259, Nov. 28, 2013.
[26] M. Perino et al.,"Comparative study of two measurement/modeling techniques for biodevices functionalization assessment in agri-food applications," *IEEE AISEM Annual Conference XVIII*, pp. 1-4, 2015.
[27] R. P. Janek et al., "Impedance Spectroscopy of Self-Assembled Monolayers on Au(111): Sodium Ferrocyanide Charge Transfer at Modified Electrodes," *Langmuir*, vol. 14, no. 11, pp. 3011–3018, 1998.
[28] A. Saltelli et al., "Sensitivity analysis practices: Strategies for model-based inference," *Reliability Engineering & System Safety*, vol. 91, Issues 10–11, pp. 1109-1125, 2006
[29] W. Franks et al., "Impedance Characterization and Modeling of Electrodes for Biomedical Applications," *IEEE Trans. Biom. Eng.* vol. 5, pp. 1295-1302, 2005.
[30] J.R. Taylor, *An Introduction to Error Analysis*. Mill Valley, CA: University Science Books, 1982.
[31] F. Matemadombo and P. Westbroek, "Immobilization of tetra-amine substituted metallophthalocyanines at gold surfaces modified with mercaptopropionic acid or DTSP-SAMs," *Electrochim. Acta*, vol. 52, no. 5, pp. 2024–2031, 2007.
[32] P. N. Bartlett, F. Pariente, M. Gamero, E. Lorenzo, M. Sosna, C. Alonso, "Influence of macroporous gold support and its functionalization on lactate oxidase-based biosensors response". *Talanta*, *94*, 328–334, 2012.
[33] M. Gamero, J. L. G. Fierro, E. Lorenzo, C. Alonso, "Electrocatalytic Activity of 3-Dimensional Ordered Macroporous Gold Electrode-Based Lactate Biosensors Platforms as a Function of Pore Layer Number". *Electroanalysis*, no. *25*(1), pp. 179–188, 2013.
[34] Kovacs, G.T.A. *Enabling technologies for cultured neural networks*, Academic Press, 1994.
[35] Scaramuzza et al., "Low-cost Enzyme-based biosensor for lactic acid amperometric detection," Proceeding of the Int. Conf. on Biomed. Electr. and Devices, pp. 380-383, 2012.
[36] M. Boujtita et al., "Enzymatic electrode for the determination of L-lactate," *Electroanalysis*, no. 5, pp. 485–488, 1996.
[37] A. Szucs et al., "On the adsorption of Glucose Oxidase at a Gold Electrode," *Journal of the Electrochemical Society*, no. 136, issue 12, pp. 3748-3755, 1989.